To the Graduate Council:

I am submitting herewith a thesis written by Peter K. Carlson entitled "Zone Method for Determining Heat Transfer and Temperature Field for a Coal-Fired MHD Combustor." I recommend that it be accepted in partial fulfillment of the requirements for the degree of Master of Science, with a major in Engineering Science.

Lloyd Crawford

Lloyd Crawford, Major Professor

We have read this thesis
and recommend its acceptance:

Y. C. L. Wu

Mary H Scott

Accepted for the Council:

L Evans Pond

Vice Chancellor
Graduate Studies and Research

Thesis
78
C3574
cop. 2

ZONE METHOD FOR DETERMINING HEAT TRANSFER AND TEMPERATURE FIELD FOR A COAL-FIRED MHD COMBUSTOR

A Thesis

Presented for the

Master of Science

Degree

The University of Tennessee, Knoxville

Peter K. Carlson

December 1978

1 [illegible]

ACKNOWLEDGMENTS

The author is grateful for the assistance, guidance and patience of Dr. Lloyd Crawford who contributed his valuable time and energy so that this work could be completed within the required time.

Recognition is given to Ronald L. Kolbe, a fellow Graduate Research Assistant, for his valuable contributions and Dr. Gabriel Roy who supplied much data in a usable form. The help of other students, engineers, and secretaries at UTSI is also appreciated.

Dr. Y.C.L. Wu and Dr. Mary Scott, who served as Committee members and gave also of their valuable time, are remembered and thanked.

Finally, appreciation is expressed to June Jarrell for her fine typing and patient cooperation in this work.

ABSTRACT

A method of estimating heat losses to the walls of a coal-fired MHD combustor and of predicting temperature distributions within the combustion flame is investigated in this work. The importance of temperature of combustion products and combustor heat losses to the MHD energy conversion process is briefly discussed in the introductory chapter. A short description of the actual combustor being modeled is presented as well as the method being used to calculate heat transfer from available data. A qualitative assessment of the factors believed to affect heat transfer and temperature in the UTSI combustor system is postulated and actual heat losses are shown graphically. Applicable background work leading to this thesis and source material of the zone method is given.

A description of the zone procedure employed in the computer program is covered in Chapter II. Geometrical considerations and the exchange area concept used in radiation heat transfer are explained first. Next follows a discussion of gas and particle radiating-absorbing systems and how emissivity is found for such systems. A method by which real gas-particle mixture emissivity can be expressed in a mathematical formulation compatible with the exchange area concept is developed. Finally, the formulation of a

heat balance for the entire system of zones with a convection contribution added is given.

Chapter III covers how the required inputs to the program are found and explains how the program is to be demonstrated for this work. Data from two combustor tests are given and used to theoretically determine possible temperature distributions within the enclosure.

Finally the resulting temperature distributions obtained from the program are discussed and the most likely sources of error are pointed out. Shortcomings of the method and suggested ways of improving it are given with estimates of relative complexity added by the improvements.

TABLE OF CONTENTS

CHAPTER		PAGE
I.	INTRODUCTION.	1
	A. The Need for a Combustor Model.	1
	B. Description of Combustor.	5
	C. Background Material and Previous Work	7
II.	ZONE METHOD FOR HEAT TRANSFER AND TEMPERATURE FIELD	11
	A. Zoning the Enclosure.	11
	B. Direct Exchange Areas	13
	C. Flame Emissivity and Absorptivity	18
	D. The Mathematical Emissivity Model	26
	E. Method of Solution.	33
III.	CALCULATIONS USING ZONE METHOD.	41
	A. Required Inputs	41
	1. Surface temperatures and emissivities.	42
	2. Gas temperatures and flame properties.	43
	B. Demonstration of the Method	46
IV.	DISCUSSION OF RESULTS	54
V.	CONCLUSIONS AND SUGGESTIONS FOR FURTHER WORK.	56
LIST OF REFERENCES.		58
VITA.		60

LIST OF TABLES

TABLE		PAGE
1.	Actual Emissivity/Value from Model.	27
2.	Variations Along Chamber Length, P = 4 (atms), E_R = 1.0 (Oxidizer: Ordinary Air at 1,900°K) . . .	44
3.	Variations Along Chamber Length, P = 4 (atms), E_R = 1.0 (Oxidizer: Pure O_2 at 298 °K)	45
4.	Run Conditions and Heat Losses for Runs 36-4 and 36-33.	47
5.	Equilibrium Thermodynamic Properties and Chemical Composition of Combustion Products for Run 36-4.	48

LIST OF FIGURES

FIGURE		PAGE
1.	Conductivity vs. Temperature for Coal Combustion Products Seeded with K_2CO_3	2
2.	Unburned Coal, Gas Temperature and Heat Transfer Ratio vs. Residence Time	4
3.	4 lb./sec. Vitiation Heater/Combustor	6
4.	Cumulative Heat Loss in the Combustor System	9
5.	Cylindrically Zoned Enclosure	12
6.	Method of Determining K_1 and a_1	30
7.	Temperature Weighting Functions	34
8.	Input Zone Temperature	50
9.	Actual and Computed Losses for Run 36-33	51
10.	Actual and Computed Losses for Run 36-4	52
11.	Theoretical Temperature Fields	53

NOMENCLATURE

A, A_i	Area.
$a_{g,i}$ or a_i	Temperature weighting coefficient of gas zone i.
$a_{s,i}$	Temperature weighting coefficient of surface zone i.
a	Total surface area of particles per unit volume of space (m^{-1}).
B	Zone sizing dimension.
C_p	Constant pressure specific heat.
D, D_i	Diameter.
dV, dA, etc.	Differential quantities.
E, E_i	Black emissive power (energy/time-area).
$\overline{ee}(a,b_1,b_2)$	Nondimensional end to end exchange area.
$\overline{ew}(a,b_1,b_2)$	Nondimensional end to wall exchange area.
E_R	Equivalence ratio $\left(\frac{\text{Theoretical oxidant}}{\text{Actual Oxidant}}\right)$.
F_{ji} or F_{ij}	Configuration factor.
FVM	Fraction volatile matter.
$\overline{G_iG_j}$ or $\overline{G_jG_i}$	Total exchange area for gas to gas exchange.
$\overrightarrow{G_iG_j}$ or $\overleftarrow{G_iG_j}$	Directed flux area for gas to gas exchange.
$\overline{G_iS_j}$ or $\overline{G_jS_i}$	Total exchange area for gas to surface exchange.

$\overrightarrow{G_iS_j}$ or $\overleftarrow{G_iS_j}$	Directed flux areas for gas to surface exchange.
$\overline{ge}(a,b_1,b_2)$	Nondimensional exchange area for gas to end exchange.
$\overline{gg}(a,b_1,b_2)$	Nondimensional exchange area for gas to gas exchange.
$\overline{gw}(a,b_1,b_2)$	Nondimensional exchange area for gas to wall exchange.
$\overline{g_ig_j}$ or $\overline{g_jg_i}$	Direct exchange area for gas to gas exchange.
h	Convection heat transfer coefficient (energy/time-area).
I	Intensity (energy/time-steradian).
I_λ, I_{o_λ}	Monochromatic intensity.
K	Absorption or extinction coefficient (length-1).
K_p	Absorption coefficient due to particles.
K_g	Absorption coefficient due to gases.
K_i	Absorption coefficient of gray gas i.
K_λ	Monochromatic absorption coefficient.
k	Gaseous thermal conductivity (energy/length-time-degree).
L, ℓ	Distance.
m_i	Initial mass.
m_f	Final mass.
$\dot{m}_c$, $\dot{m}_{seed}$, $\dot{m}_{kerosene}$ $\dot{m}_{O_2}$, $\dot{m}_{N_2}$, $\dot{m}_{total}$	Mass flows (mass/time).

P	Total pressure.
Pr	Prandtl number.
p_c, p_w, p_g	Partial pressures of individual gases.
PVM	Percent volatile matter.
$\dot{Q}$	Heat transfer (energy/time).
q	Heat flux (energy/time area).
r_i	Initial radius.
r_f	Final radius.
r	Distance between differential elements.
Re	Reynolds number.
R_i	Reflected flux from zone i.
$\overline{S_iS_j}$ or $\overline{S_jS_i}$	Total exchange area for surface to surface exchange.
$\overleftarrow{S_jS_i}$ or $\overrightarrow{S_jS_i}$	Directed flux area for surface to surface exchange.
$\overline{s_is_j}$ or $\overline{s_js_i}$	Direct exchange area for surface to surface exchange.
$\overline{s_ig_j}$ or $\overline{s_jg_i}$	Direct exchange area for surface to gas exchange.
T	Temperature.
T_g	Gas temperature.
T_s	Surface temperature.
ΔT	Temperature change.
t	Reduced temperature ($^oK/1000$).
t_r	Residence time.

V, V_i	Volume.
V_c	Volume of combustor.
W, W_i	Leaving flux.
$\overline{ww}(a,b)$	Nondimensional wall to wall exhchange area.

Greek Symbols

α_{gs}	Gaseous absorptivity at surface temperature.
α_λ	Monochromatic absorptivity.
δ_{ij}	Kronecker delta.
λ	Wavelength.
ε	Emissivity.
ε_g	Gas emissivity.
ε_p	Particle emissivity.
ε_λ	Monochromatic emissivity.
ε_T	Total emissivity.
ρ_s, $\rho_{s,i}$	Surface reflectivity.
ρ_i	Initial density.
ρ_f	Final density.
$\tau(r)$	Transmitted fraction.
θ	Angle.

CHAPTER I

INTRODUCTION

A. The Need for a Combustor Model

Magnetohydrodynamic (MHD) energy conversion requires that combustion of fuel be carried out at temperatures much higher than those of existing fossil fuel power plants, creating a unique set of problems currently under study at The University of Tennessee Space Institute (Energy Conversion Division). These higher temperatures are necessary to ensure sufficient seed ionization, thus electrical conductivity, of the combustion products. The graphs of Figure 1 [1][1] illustrate conductivity versus temperature for the combustion products of pulverized coal burned in preheated air with potassium carbonate (K_2CO_3) as seed and at various pressures. Combustion pressures should be in the range of 5 atm. and conductivity channel pressures about 3 atm. so that a desired conductivity of 10-25 mhos/meter will necessitate temperatures higher than 2800K. A proper balance between factors influencing combustion and heat transfer must be maintained to achieve good ionization with tolerable losses in combustion devices. It becomes desirable to build devices as close to adiabatic

[1]Numbers in brackets refer to similarly numbered references in the List of References.

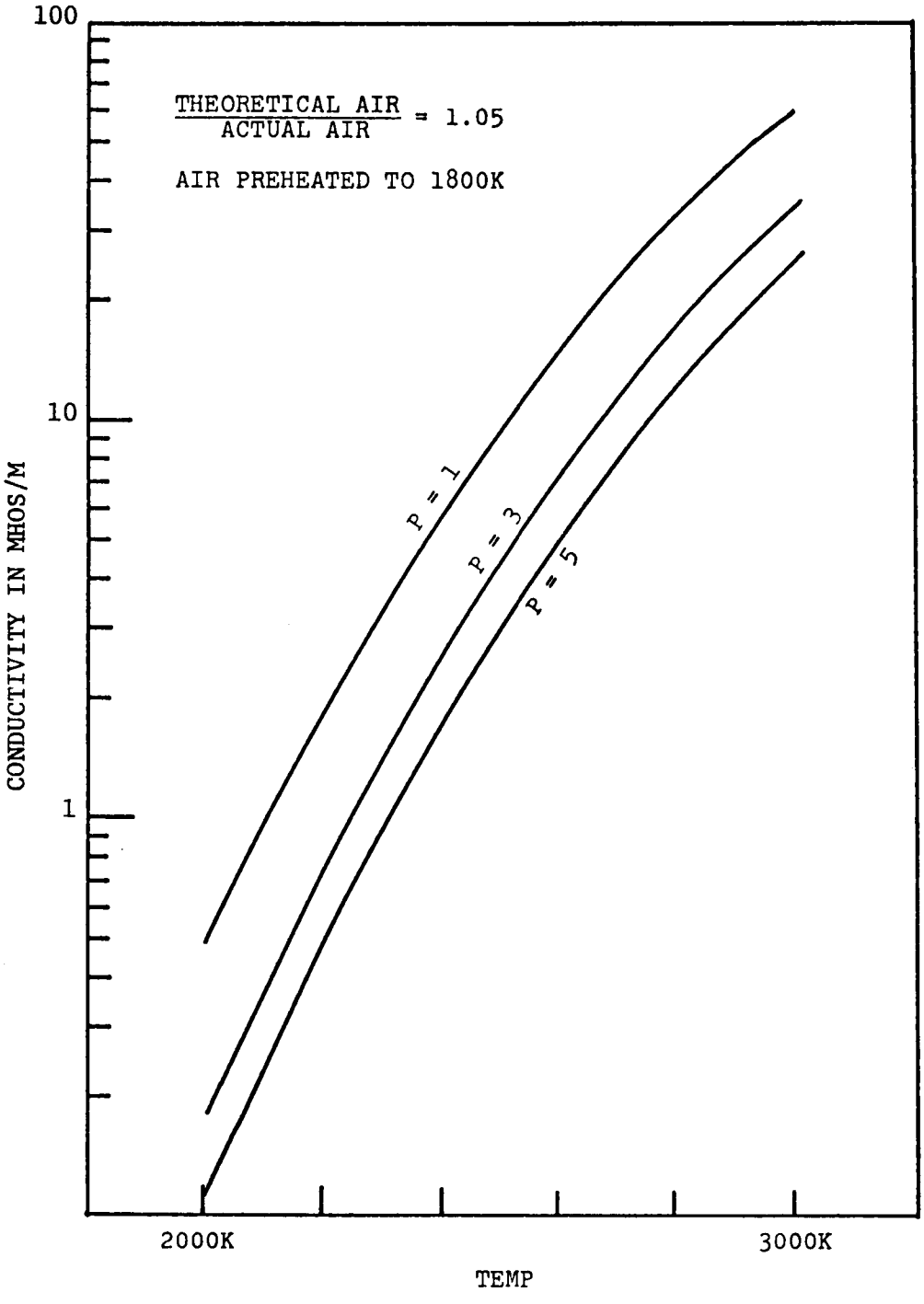


Figure 1. Conductivity vs. Temperature for Coal Combustion Products Seeded with K_2CO_3.

as possible with proper consideration given to required combustion residence time and other relevant parameters (Figure 2 [2,9]). Material selection, shape and cooling requirements must be determined for optimum designs and the complicating factors of slag deposition and carry-over, and corrosion of lining materials have to be considered.

What is needed is the capability to predict the rates of heat transfer and temperature distributions in MHD combustion devices and other flow train components.

It was chosen to model the 4 lb./sec. total mass flow vitiation heater-combustor, currently undergoing testing and evaluation at The University of Tennessee Space Institute (UTSI), since heat transfer data is available over a number of tests with different input conditions for this device. As the device is water cooled, the heat transfer rates are routinely calculated as follows:

$$\dot{m}_{water}\, C_{p_{water}}\, \Delta T_{water} = \dot{Q}_{combustor} \qquad (1.1)$$

where

$\dot{m}_{water}$ = cooling water flow rate,
$C_{p_{water}}$ = heat capacity of water,
ΔT_{water} = temperature rise of cooling water from inlet to outlet.

However, it is much more difficult to determine the temperature distribution of combustion products within the

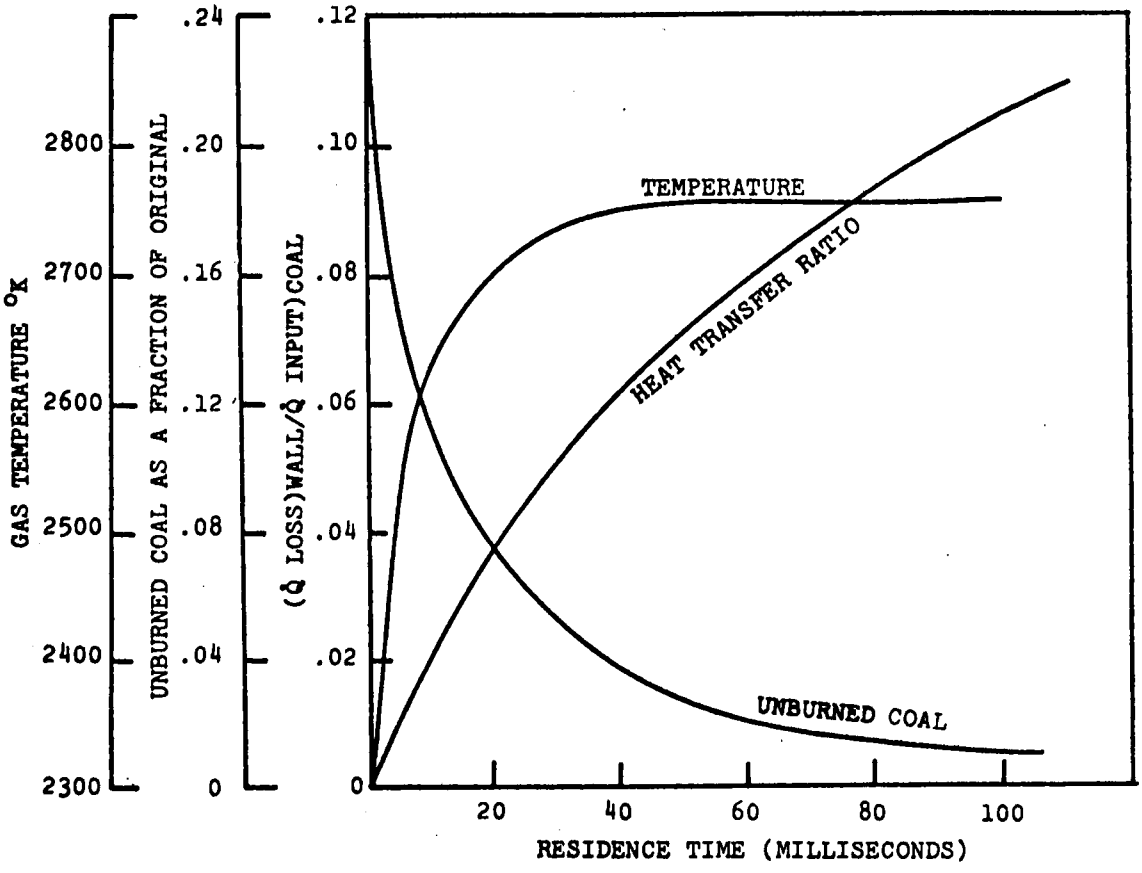


Figure 2. Unburned Coal, Gas Temperature and Heat Transfer Ratio vs. Residence Time.

device, since the high temperatures, corrosive and slagging conditions render ordinary measuring techniques impractical. In future design work where the problems of scaling up for commercialization ultimately must be faced, a computer program capable of predicting heat transfer rates and temperatures would be a useful tool.

B. Description of Combustor

The device shown in Figure 3 is the 4 lb./sec. vitiation heater-combustor currently being tested at UTSI. At the upstream end is a small cylinder followed by a larger coaxial cylinder. In these sections kerosene is burned with excess oxygen and the products are further mixed with nitrogen. The resulting mixture simulates preheated air. The next cylindrical section provides for thorough mixing and is followed by the coal combustor and a converging conical section. Further downstream is a nozzle and the generator channel (neither is shown in Figure 3). The only portion of the vitiation heater-combustor assembly that is included in this study is the cylindrical coal combustor with an approximation of at least the upstream portion of the converging conical section added as a result of zone sizing limitations which are discussed in the section on zoning.

In some tests a perforated plate was installed between the two cylindrical sections at the location of the

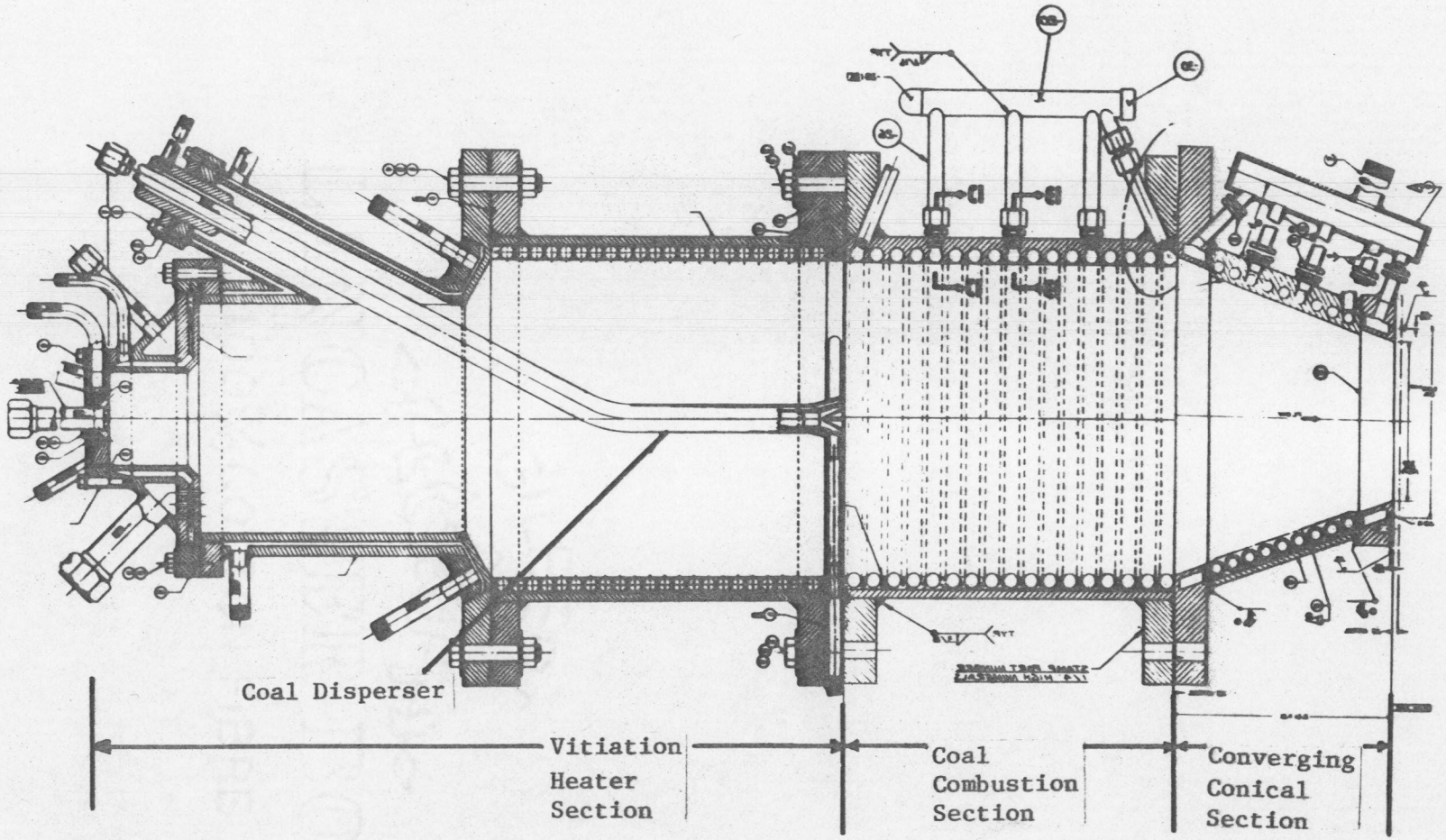


Figure 3. 4 lb./sec. Vitiation Heater/Combustor.

coal dispersing tube exit. The plate was added to facilitate mixing and to improve combustion. One test has been carried out with a cylindrical extension placed between the combustor and conical sections in order to increase residence time of fixed carbon.

The walls of the combustor are lined with cooling coils (stainless steel water tubes) embedded within a refractory material. The outer shell is constructed of stainless steel. During operation liquid slag is known to coat the inside walls of the combustor and other downstream surfaces. Inspection of combustor walls following tests have revealed that some areas of the combustor and conical sections have lost virtually all of the refractory lining material down to the tube surfaces and only a thin layer of solid slag remains to cover the water tubes.

C. Background Material and Previous Work

The zone heat transfer and temperature field procedure as well as the mathematical emissivity model and much of the experimental emissivity data used here are taken from the reference and textbook by H. C. Hottel and A. F. Sarofim entitled "Radiative Transfer" [3]. The Ph.D. dissertation presented by Balbir Arora, a former student and researcher at UTSI, and entitled "A Mathematical Model of a Pulverized Coal Fired Combustion Chamber" [4], served

as a starting place for this work. Arora used a simplified approach for calculating heat transfer, neglecting energy exchange in the axial direction. His goal was not so much to determine precise heat flux or temperature distributions but rather gross losses and expected exit temperatures. He suggested that further work be done in this area and this work is the next step to a more comprehensive three-dimensional thermodynamic-flow model of the MHD combustion process.

Heat transfer from the device under consideration has been found to be highly dependent on the degree of mixing between the coal stream and the vitiated air stream. For example, when the perforated plate was installed, heat transfer from the cylindrical and conical sections increased substantially over runs conducted without the plate. A graph [5] showing typical cumulative heat loss versus axial position for the whole combustor assembly is shown in Figure 4. The figure also shows losses for the same configuration with one type of perforated plate device installed. It is suggested that improved turbulent mixing of fuel and oxidant created higher temperatures, thus accounting for higher heat transfer rates. Any three-dimensional model used for prediction of a temperature and heat flux distribution will need as input information the quantity of fuel available for combustion within any given zone--in other words, a flow model. The NASA computer

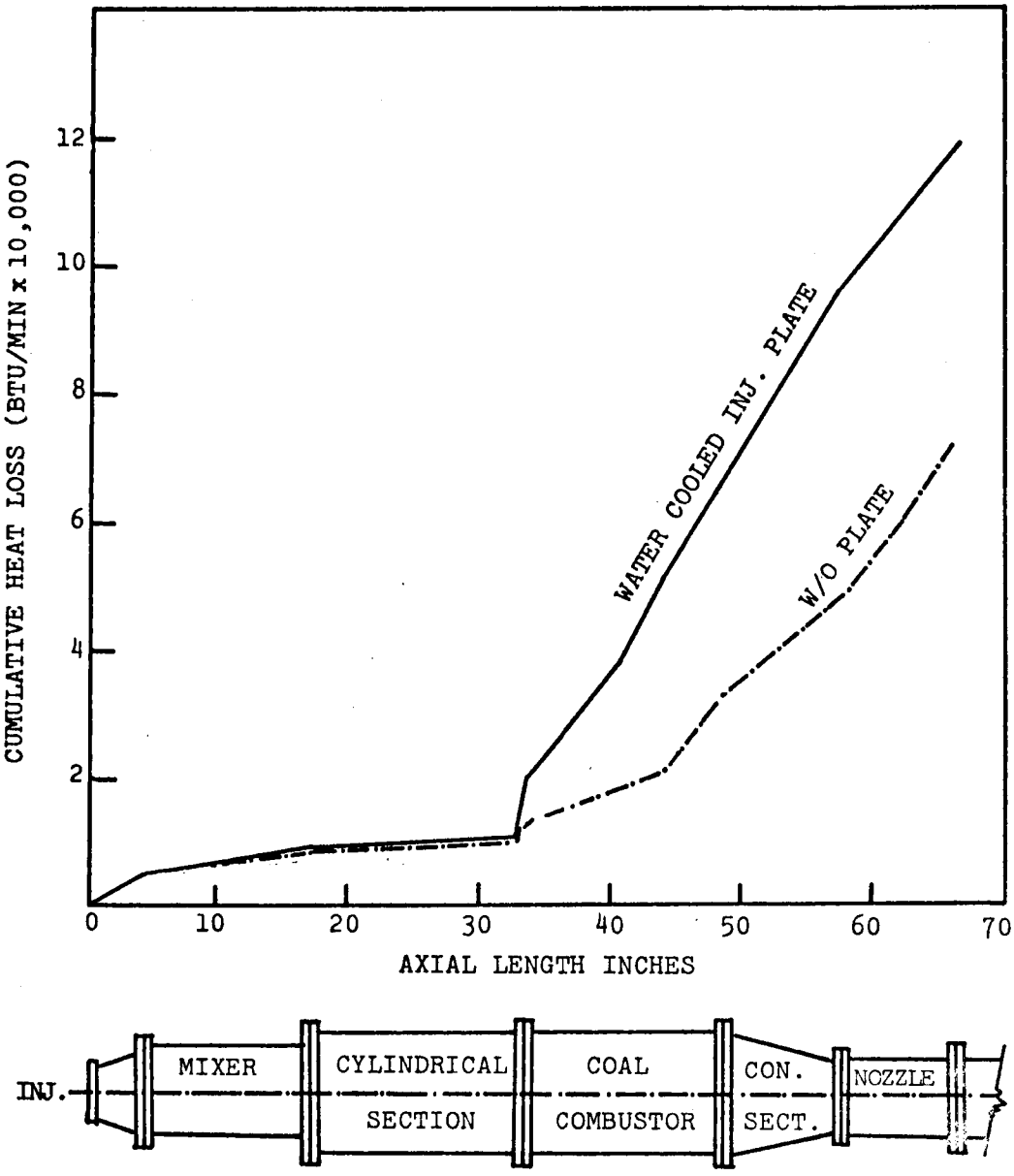


Figure 4. Cumulative Heat Loss in the Combustor System.

program, Reference [1], is widely used by UTSI personnel for obtaining adiabatic flame temperatures, compositions and other properties of the combustion products and could be used in conjunction with a flow model and zone heat transfer model to complete the combustion model. Unfortunately, no adequate flow model is available at this time and therefore simplifying assumptions are made when needed. These assumptions will be treated in subsequent sections.

CHAPTER II

ZONE METHOD FOR HEAT TRANSFER AND TEMPERATURE FIELD

A. Zoning the Enclosure

A cylinder filled with hot gases and particles, with symmetric temperature distribution about the axis, is being considered. The cylindrical flame and its envelope are divided into surface and volume zones with the grid shown in Figure 5. Within any given zone the temperature is assumed uniform as are the radiating properties of the absorbing-emitting medium. Energy exchange between all possible pairs of zones (gas to gas, gas to surface, surface to surface) is permitted by radiation, and exchange by convection between the outer volume and adjacent surface elements is allowed.

Let "B" be the characteristic dimension of the grid, corresponding to either a unit of radius or a unit of axial length. The actual dimensions of the cylindrical section are (15" axial x 14" dia.) so that if B is set equal to 1/2 the radius, 5 sections of axial length will give some extra length over the actual device. To achieve realistic numerical results the input information for this section, due to deviation from actual size and shape, and the end zones because of the fact that they are only imaginary

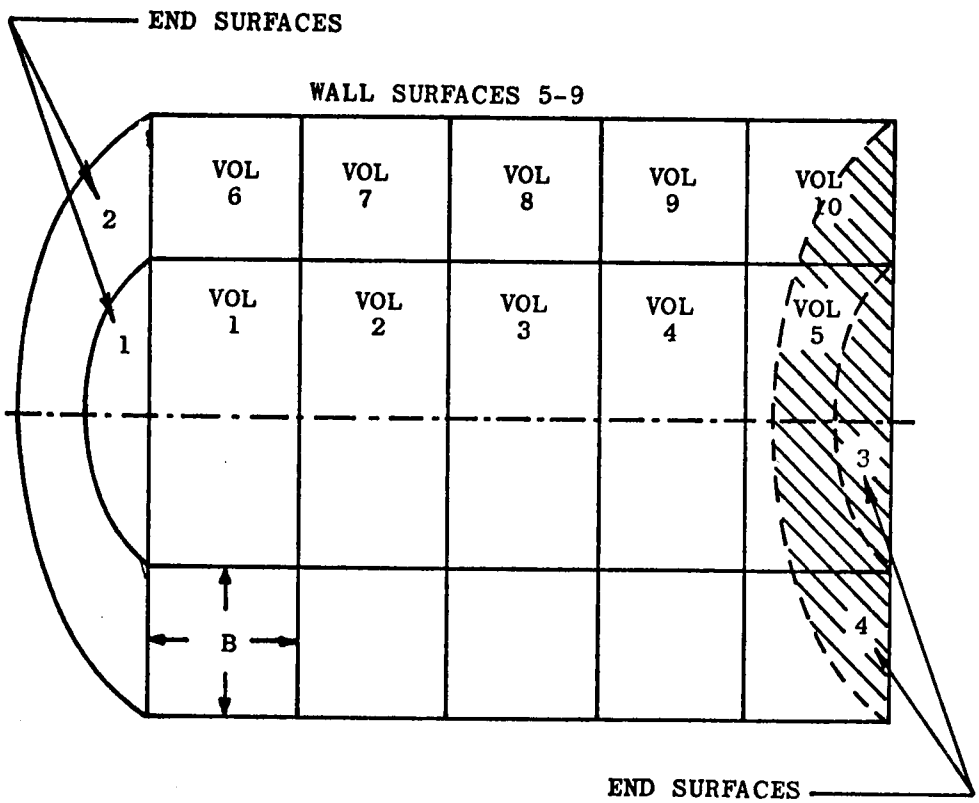


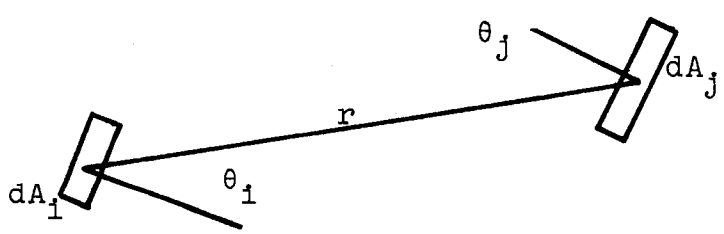
Figure 5. Cylindrically Zoned Enclosure.

surfaces, will require that some assumptions be made. Also, the results for these regions will require some judicious interpretation in their application.

This relatively simple grid has been chosen in order to demonstrate the method, with the understanding that smaller, more numerous divisions would increase confidence in the solutions.

B. Direct Exchange Areas

The problem of radiative exchange within an enclosure containing a participating medium is more difficult than an evacuated enclosure problem of the same geometry. This difficulty arises in the determination of something analogous to configuration factors. The evacuated enclosure problem deals only with surface-to-surface exchange where an elemental exchange between a black surface element i and element j would be as follows:



$$E/\pi \; dA_i \cos\theta_i \times dA_j \cos\theta_j / r^2 = d\dot{Q}_{i \to j} \qquad (2.1)$$

where

$E/\pi \; dA_i \cos\theta_i$ = emission in direction θ_i, per unit solid angle;

$dA_j \cos\theta_j / r^2$ = solid angle subtended by dA_j at dA_i;

$d\dot{Q}_{i \to j}$ = flux leaving A_i which is intercepted at A_j;

E is called the black emissive power, and

$$E = \sigma T^4 \quad ;$$

σ is the Stefan-Boltzmann constant;

T is absolute temperature.

If the enclosure is, however, filled with an absorbing medium, a substance which attenuates the propagating flux, then the second term on the left in Equation (2.1) is multiplied by a factor $\tau(r)$ which is the transmitted fraction. $\tau(r)$ depends on the transmitting medium, specifically, its absorption properties and is defined mathematically as follows:

$$\tau(r) = \exp\left[- \int_0^r K \, dr \right] \tag{2.2}$$

where K is called the absorption or extinction coefficient. A clear gas is one where K approaches zero, thus τ approaches unity. A cloud of large K is optically dense. A gray gas is one where the idealization of uniform K across the wavelength spectrum holds.

Unlike the evacuated enclosure problem, a differential volume of space within the gas-filled enclosure

acts in much the same manner as a surface element, exchanging energy with other volumes and surface elements. For example, a volume to surface flux would be given by

$$4KdVE \times dA \cos\theta/4\pi r^2 \times \tau(r) \tag{2.3}$$

where

$4KdVE$ = emission by dV in 4π steradians,

$dA \cos\theta/4\pi r^2$ = fraction directed towards dA.

A volume to volume exchange would be calculated,

$$QdV_i \cdot dV_j = \frac{K_i \, dV_i \, K_j \, dV_j \, \tau(r) \, E_i}{\pi r^2} \quad . \tag{2.4}$$

Let the following terms be defined as follows:

$$\overline{s_i s_j} = \frac{\dot{Q}_{i \not\geq j}}{E_i - E_j} = \int_{A_i} \int_{A_j} \frac{dA_i \cos\theta_i \, dA_j \cos\theta_j \, \tau(r)}{\pi r^2} , \tag{2.5}$$

$$\overline{g_i s_j} = \frac{\dot{Q}_{i \not\geq j}}{E_i - E_j} = \int_{V_i} \int_{A_j} \frac{K_i \, dV_i \, dA_j \cos\theta_j \, \tau(r)}{\pi r^2} , \tag{2.6}$$

$$\overline{g_i g_j} = \frac{\dot{Q}_{i \not\geq j}}{E_i - E_j} = \int_{V_i} \int_{V_j} \frac{K_i \, dV_i \, K_j \, dV_j \, \tau(r)}{\pi r^2} \quad . \tag{2.7}$$

The three preceding newly defined quantities are called direct exchange areas for surface to surface, gas to surface, and gas to gas exchange, respectively. When dealing with configuration factors the following

relationship holds:

$$A_i F_{ij} = A_j F_{ji} \quad ,$$

known as the reciprocity rule. For exchange areas, the analogous rule is

$$\overline{s_i s_j} = \overline{s_j s_i} \quad , \tag{2.8}$$

$$\overline{g_i s_j} = \overline{s_j g_i} \quad , \tag{2.9}$$

and

$$\overline{g_i g_j} = \overline{g_j g_i} \quad . \tag{2.10}$$

Similarly, the rule of configuration factor algebra that

$$\sum F_{ij} = 1$$

can be compared to the rule for direct exchange areas,

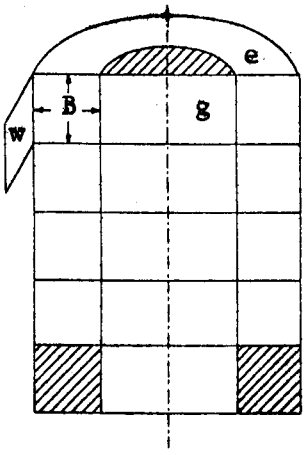
$$\sum_i \overline{s_i s_j} + \sum_i \overline{g_i s_j} = A_j \quad , \tag{2.11}$$

and

$$\sum_i \overline{g_i g_j} + \sum_i \overline{g_j s_i} = 4KV_j \quad . \tag{2.12}$$

Thus direct exchange areas are used in much the same manner as configuration factors with the important difference that while the latter is dimensionless, the former has dimensions of area.

A complete set of exchange areas for the cylindrical grid previously discussed can be found in Reference [3]. They have been calculated for various values of KB, the product of absorption coefficient and characteristic dimension. Below is a chart showing how they are referenced for use in a numerical calculation procedure.



a = maximum axial distance between zones (multiple of "B")

b_1 = maximum distance from axis of zone 1 (multiple of "B")

b_2 = maximum distance from axis of zone 2 (multiple of "B")

There are six possible combinations of e (end zone), w (wall zone) and g (gas zone). They are:

$\overline{ww}(a,b)$ [1]

$\overline{gw}(a,b_1,b_2)$

$\overline{ew}(a,b_1,b_2)$

$\overline{gg}(a,b_1,b_2)$

$\overline{ee}(a,b_1,b_2)$

$\overline{ge}(a,b_1,b_2)$

---

[1] Only one radial distance is required since the radius of a cylinder is constant.

As an example, the direct exchange area between the two shaded zones would be found by multiplying $\overline{ge}(5,2,1)$ by the appropriate function of K and B.

C. Flame Emissivity and Absorptivity

The emissivity of a combustion cloud is difficult to determine with high accuracy by any means other than direct measurement. The emissivities which are determined here are ultimately to be used in the formulation of a mathematical model. This model will yield one or more gray gas absorption coefficients and a temperature weighting function for each coefficient. The model will enable the determination of a quantity called the directed flux area, discussed later.

Emissivities and absorptivities used in the model are to include gaseous and particulate contributions, since both will subsequently be shown to be significant in the pulverized coal flames. The gaseous contribution will be considered first.

Combustion gases such as carbon dioxide and water vapor absorb and emit in discrete wavelength bands while remaining essentially non-responsive in other portions of the spectrum. The functional form for a gaseous emissivity is given by

$$\varepsilon_g = \varepsilon(T_g, P_g, P, L) \tag{2.13}$$

where

T_g = gas temperature

P_g = partial pressure of the gas

P = total pressure of all gases

L = path length

This is the total emissivity and has been integrated over the whole spectrum. When two or more gases are present together the discrete bands become more numerous, different effects cause the bands to broaden, and the mixture tends to behave more as a gray gas (emissivity less dependent on wavelength). The emissivity of a mixture of water vapor, carbon dioxide, carbon monoxide, and other essentially non-participating gases such as nitrogen and oxygen, can be estimated by combining the individual emissivities and applying certain experimentally determined corrections. Experimentally measured gas emissivities and the appropriate mixture corrections are given in References [3] and [6]. For determining emissivity of combustion gas mixtures at various pressures a computer program, written by Ronald L. Kolbe [7] and utilizing the data in a system of curve fits, has been used. The program has been included as a subroutine, with some modifications, into the heat transfer program for this thesis.

When considering a radiation source at one temperature and a gaseous absorbing sink at another,

it is necessary to know the absorptivity of the gas at the source temperature, denoted by α_{gs}. This is because the wavelength distribution of the propagating radiation is a result of the surface emission while the absorptive properties of the gas depend on the temperature of the gas. When the source temperature equals the gas temperature then α_{gs} is equal to ε_g, but this is not normally the case. Reference [3] gives emissivity-absorptivity correlations for the two most prevalent participating component gases of combustion, carbon dioxide and water vapor. For CO_2,

$$\alpha_{gs}(T_g,T_s,P_c,L) = \left(\frac{T_g}{T_s}\right)^{0.65} \varepsilon_g\left(T_s,P_c\ L\ \frac{T_s}{T_g}\right) \quad , \qquad (2.14)$$

and for H_2O,

$$\alpha_{gs}(T_g,T_s,P_w,L) = \frac{T_g}{T_s}^{0.45}\ \varepsilon_g\left(T_s,P_w\ L\ \frac{T_s}{T_g}\right) \quad . \qquad (2.15)$$

For the sake of simplicity, T_g is to be chosen as some average gas temperature and α_{gs} allowed to vary with Ts.

Coal particles in various stages of combustion are also present in the flame, and their contributions to total flame emissivity must be considered. While an estimate of gaseous composition of combustion products can be obtained through the use of the NASA computer code, Reference [1], very little is known about combustion histories of coal particles or how particle size is

affected by devolatilization and burning of fixed carbon. For this reason a simplified model has been developed. A short discussion on emissivity of a cloud and how it is related to the absorption coefficient is discussed here.

The attenuation $-dI_\lambda$ due to absorption of a beam of collimated monochromatic radiation of intensity I_λ upon passage through a differential slab of thickness $d\ell$ is proportional to the intensity and path length traversed, i.e.,

$$-dI_\lambda = K_\lambda I_\lambda d\ell \quad . \tag{2.16}$$

If the beam is incident on a slab of thickness L with intensity I_{o_λ}, integration of the above equation yields the attenuation law,

$$I_\lambda = I_{o_\lambda} e^{-K_\lambda L} \quad , \tag{2.17}$$

if K is independent of position. Since a blackbody of thickness L would absorb all incident radiation, then

$$\varepsilon_\lambda = \alpha_\lambda = \frac{\text{attenuation of incident radiation}}{\text{attenuation by a blackbody}}$$

$$= \frac{I_{o_\lambda} - I_\lambda}{I_{o_\lambda}}$$

$$= 1 - e^{-K_\lambda L} \quad . \tag{2.18}$$

For a gray gas and black particle mixture, where K is independent of λ, and the intensity has been integrated over all wavelengths,

$$I = I_o e^{-(K_p + K_g)L} \tag{2.19}$$

where

K_p = particle absorption coefficient

K_g = gray gas absorption coefficient

Then

$$\varepsilon_T = 1 - e^{-(K_p + K_g)L} \tag{2.20}$$

$$1 - \varepsilon_T = e^{-K_p L} \, e^{-K_g L} \tag{2.21}$$

$$1 - \varepsilon_T = (1 - \varepsilon_p)(1 - \varepsilon_g) \tag{2.22}$$

This result demonstrates that the total emissivity of a flame can be determined by calculating the gaseous contribution and particle contributions separately, and combining according to Equation (2.22).

Particle emissivity is calculated by finding the particle absorption coefficient, K_p. The units on K_p are inverse length and arise from the fact that it represents an effective area of interception by particles per unit volume swept out by the radiation beam. This quantity is, in general, difficult to evaluate since in a real situation

the particles would be different sizes, shapes, surface roughness, and so forth. For simple black spherical particles K_p is equal to the total cross-sectional area of particles per unit volume of space, but, in general, K_p equals $a/4$, where a equals the total surface area per unit volume of space. In a simplified approach used here, the particles are assumed to be black spherical radiators of a single diameter. The pulverized coal, as fed to the combustor, has a known particle size distribution so that a mean diameter may be calculated. The composition of the coal is assumed to be uniform and in known proportions of fixed carbon, volatile matter and ash.

Let m_i equal the average mass of an incoming particle. As the stream of particles enters the hot combustor, rapid heating liberates volatile species and the mass of the particles is reduced by the amount of volatile matter released. Since devolatilization has been found to occur much more rapidly than combustion of fixed carbon, it will be assumed that the particles lose that portion of their mass instantaneously upon entry into the chamber. Therefore, if

m_f = mass of devolatilized particle

FVM = fraction volatile matter

then

$$m_f = m_i(1 - FVM) \tag{2.23}$$

Let

A = surface area of devolatilized particle,

ρ_i = initial density of coal particle,

ρ_f = density of devolatilized coal particle,

r_i = initial particle radius,

r_f = devolatilized particle radius,

D_i = initial particle diameter.

Then,

$$m_i = \rho_i\left[\frac{4}{3}\,\pi r_i^{\,3}\right] \quad ,$$

and

$$m_f = \rho_f\left[\frac{4}{3}\,\pi r_f^{\,3}\right] = [1 - FVM]\rho_i\left[\frac{4}{3}\,\pi r_i^{\,3}\right] \quad .$$

Thus,

$$r_f = \left[(1 - FVM)\,\frac{\rho_i}{\rho_f}\right]^{1/3} r_i \tag{2.24}$$

and

$$A = 4\pi r_f^{\,2} = 4\pi\left[(1 - FVM)\,\frac{\rho_i}{\rho_f}\right]^{2/3} r_i^{\,2}$$

$$= \pi\left[(1 - FVM)\,\frac{\rho_i}{\rho_f}\right]^{2/3} D_i^{\,2} \tag{2.25}$$

Now, by definition,

$$a = \left(\frac{\text{no. of particles}}{\text{unit volume}}\right) A \quad . \tag{2.26}$$

The number of particles per unit volume of enclosure at any given time, assuming the incoming particles do not break apart or form into clusters, is given by

$$\frac{\text{no. of particles}}{\text{unit volume}} = \frac{\text{coal flow rate x residence time in chamber}}{\text{volume of chamber x } m_i} .$$

Let

t_r = residence time in combustion chamber,

$\dot{m}_c$ = coal mass flow rate,

V_c = volume of combustion chamber;

then

$$a = \left(\frac{\dot{m}_c t_r}{V_c m_i}\right) A \quad , \tag{2.27}$$

$$a = \left(\frac{\dot{m}_c t_r}{V_c \frac{\pi}{6} D_i^3 \rho_i}\right) \pi \left[(1 - FVM) \frac{\rho_i}{\rho_f}\right]^{2/3} D_i^2$$

$$= 6\left(\frac{\dot{m}_c t_r}{V_c D_i \rho_i}\right) \left[(1 - FVM) \frac{\rho_i}{\rho_f}\right]^{2/3} . \tag{2.28}$$

For a given set of run conditions, that is, coal flow rate, combustion pressure, and so forth, it is now possible to tabulate flame emissivity as a function of path length

and temperature by combining ε_p with ε_g or α_{gs}. Table 1 gives the emissivity of a specific mixture of gases and particles as a function of temperature and path length, where the values were obtained with the computer program utilizing the preceding methods, data and concepts.

D. The Mathematical Emissivity Model

For a gray gas, the following equation relates to K and L:

$$\varepsilon = 1 - e^{-KL} \tag{2.29}$$

For a mixture of real gases and particles it is possible to approximate the emissivity (absorptivity) as a sum of gray gases with a clear component to cover portions of the spectrum where significant emission (absorption) of radiation does not occur. The model used is of the following form:

$$\varepsilon_g(T_g, L) = \sum_i a_{g,i}(T_g)\left(1 - e^{-K_i L}\right) \tag{2.30}$$

or

$$\alpha_{gs}(T_g, T_s, L) = \sum_i a_{s,i}(T_g, T_s)\left(1 - e^{-K_i L}\right) \tag{2.31}$$

where the summation includes one K, corresponding to the clear component, equal to zero. The pressure dependency has not been included in these functional forms since

TABLE 1

ACTUAL EMISSIVITY/VALUE FROM MODEL

L Tg	5 CM	10 CM	20 CM	50 CM	100 CM
1200K	.286	.430	.608	.843	.959
	.254	.418	.608	.843	.968
1400K	.248	.386	.571	.826	.954
	.229	.382	.571	.826	.968
1600K	.217	.350	.536	.807	.948
	.206	.349	.536	.807	.961
1800K	.194	.323	.507	.789	.942
	.187	.323	.507	.789	.952
2000K	.176	.299	.482	.772	.936
	.171	.299	.482	.772	.943
2200K	.159	.277	.458	.757	.931
	.156	.278	.458	.757	.935
2400K	.144	.257	.437	.731	.926
	.143	.259	.437	.731	.928
2600K	.132	.242	.420	.731	.921
	.133	.244	.420	.731	.919
2800K	.124	.231	.407	.719	.915
	.125	.232	.407	.719	.909
3000K	.119	.223	.397	.710	.911
	.119	.224	.397	.710	.901

it has been stated that the data used will pertain to a specific set of run parameters, thus it is implicit in the equations. Since the direct exchange areas and the total exchange areas correspond to a gray gas of constant K, a complete set will have to be calculated for each term of the above series. To keep calculation time under control, it is advisable to limit the number of terms to, say, two non-zero K_i and one K equal to zero. In general, a satisfactory fit to the data, over a wide range of temperatures and path lengths, is obtainable with this relatively simple model.

For all temperatures in Eq. (2.30), ε_g is an increasing function of L, approaching unity in the limit; therefore as $L \to \infty$,

$$\varepsilon_g \to \sum a_{g,i} \to 1 \quad . \tag{2.32}$$

The procedure for determining K_1, K_2 and the temperature weighting functions follows. Suppose $K_1 << K_2$, then at large L and some fixed representative gas temperature Eq. (2.30) becomes

$$\varepsilon_g = a_{g,1}\left(1 - e^{-K_1 L}\right) + a_{g,2} \tag{2.33}$$

or

$$\frac{a_{g,1} + a_{g,2} - \varepsilon_g}{a_{g,1}} = e^{-K_1 L} \tag{2.34}$$

or

$$\ell n(a_{g,1} + a_{g,2} - \varepsilon_g) - \ell n\, a_{g,1} = - K_1 L \quad . \tag{2.35}$$

The quantity on the left is a linear function of L at large L's so that

$$\frac{d\ \ell n(a_{g,1} + a_{g,2} - \varepsilon_g)}{dL} = - K_1 \tag{2.36}$$

When $a_{g,1} + a_{g,2}$ are properly chosen the slope of $\ell n(a_{g,1} + a_{g,2} - \varepsilon_g)$ versus L will be constant and equal to $- K_1$ at large L. The procedure will be then to vary $(a_{g,1} + a_{g,2} - \varepsilon_g)$ until the above condition is satisfied to yield K_1. $a_{g,1}$ would then be figured by starting from the value for $(a_{g,1} + a_{g,2} - \varepsilon_g)$ at large L and extrapolating to L = 0 using the new K_1. From Eq. (2.35) at L = 0,

$$a_{g,1} = (a_{g,1} + a_{g,2} - \varepsilon_g) \quad . \tag{2.37}$$

Note that this would not be the same as extrapolating from the actual $(a_{g,1} + a_{g,2} - \varepsilon_g)$ data at small L since for small L the slope is not linear. The method is shown graphically in Figure 6. Note that semi-log graph paper gives a straight line slope of the quantity $(a_{g,1} + a_{g,2} - \varepsilon_g)$ versus L when $a_{g,1} + a_{g,2}$ have been chosen correctly. K_2 and $a_{g,2}$ can be determined in a similar manner now that K_1 and $a_{g,1}$ are known, and K_2 should indeed turn out to be much larger than K_1 . The size of K_2 poses a problem if

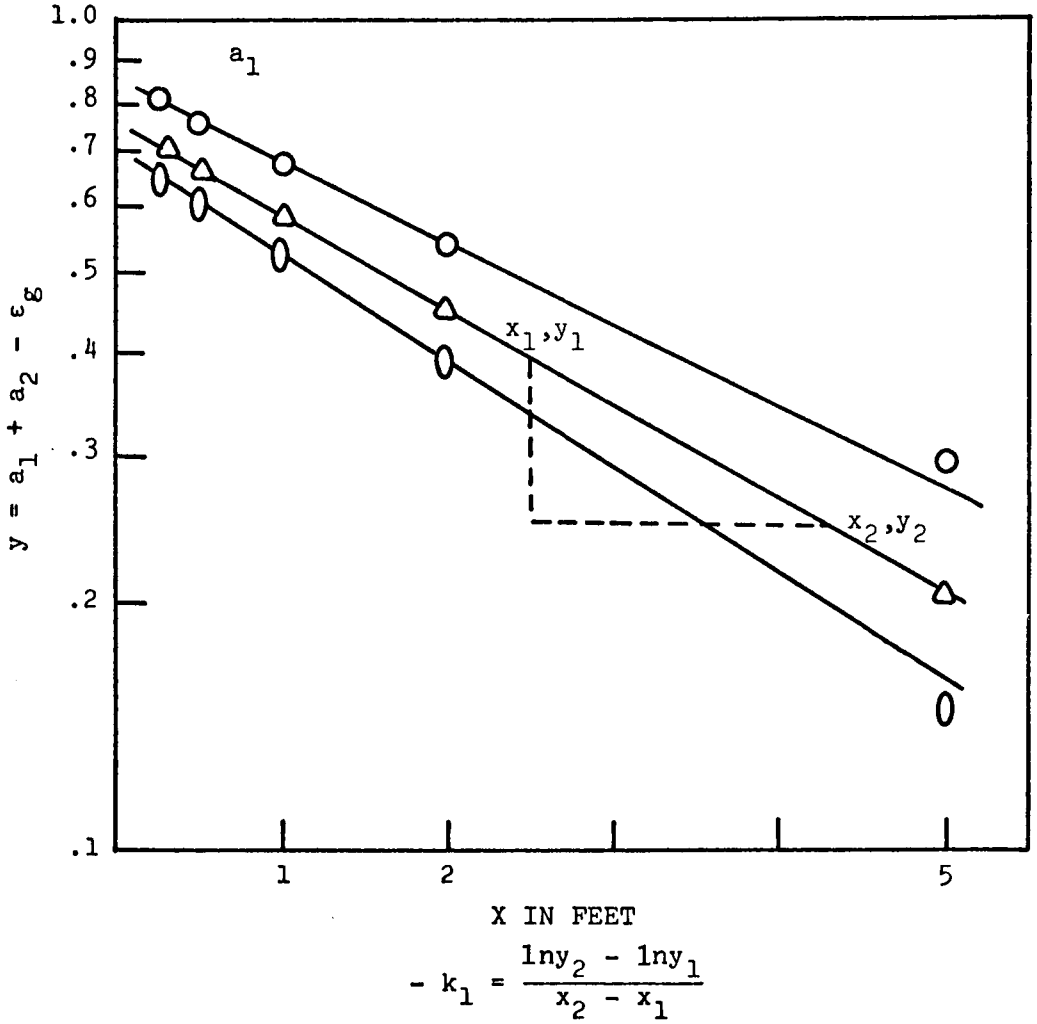


Figure 6. Method of Determining K_1 and a_1 .

the exchange area data tabulated in Reference [3] are to be used. The exchange areas are listed for KB from 0 to 1.25. The characteristic dimension chosen for the zones sets the upper limit on K if these data are to be utilized. It is found that if K_1 is figured as above and then K_2 is set to the maximum available, the emissivity model thus obtained is accurate within ±5 percent over most of the temperature range and ±10 percent for the whole range. Theoretically, of course, a three, four or more term series with no limitation on K could be made to fit as close as desired to the empirically determined curve. For comparison purposes, the empirical data and the model results have been tabulated in Table 1 for a specified particle-gas mixture.

Now that K_1 and K_2 have been determined for a representative gas temperature, it is assumed they remain constant over the whole temperature range (being dependent only on gas pressures, particle sizes, etc.) and the full burden of the temperature dependence of emissivity is borne by the $a_{g,i}$ coefficients. Since for each temperature there are two $a_{g,i}$ in the emissivity equation, two path lengths can be fit exactly to the actual data. One is chosen to be close to a representative dimension of the flame, such as the diameter of the enclosure, and the other twice the first. From the calculations tabulated in Table 1 it can be seen that 20 and 50 cm were chosen in

this case. In the final version of the computer program, 50 and 100 cm are used to determine $a_{g,1}$ and $a_{g,2}$ for the gas at each temperature. The error at small path lengths is probably worsened by the limitation on K_2, since an error in its choice would show up increasingly as path length was shortened [see Eq. (2.30)]. The following example will serve to illustrate how the $a_{g,i}$ function in the model.

A particular mixture of CO_2 and H_2O and N_2 at 5 atm. total pressure is determined to behave according to the equation

$$\varepsilon_g = a_{g,1}(1 - e^{-1.272L}) + a_{g,2}(1 - e^{-12.500L}) \quad .$$

It is found that at 2000K, $a_{g,1} = .4263$ and $a_{g,2} = .0359$. This means that 42.63 percent of the mixture acts like gray gas 1, 3.59 percent acts like gray gas 2, and the remaining 53.78 percent is the clear component, making $a_{g,3} = .5378$. For the same mixture containing a specified concentration and size of black spherical particles it is found that the emissivity fits the equation

$$\varepsilon_g = a_{g,1}(1 - e^{-2.628L}) + a_{g,2}(1 - e^{-12.500L}) \quad .$$

However, since black particles emit independently of wavelength there are no real windows in the spectral curve and hence, $a_{g,1} = .9259$, $a_{g,2} = .0670$ and $a_{g,3} = .0071$. The

addition of particles virtually eliminates the clear component. After $a_{g,1}$ and $a_{g,2}$ are found for a number of temperatures covering the range of interest, they can be fitted to a polynomial or other equation in the variable T. For the computer program here 10 temperatures were fitted over 3 ranges as shown in Figure 7 (the data used is for the case of Table 1, page 27). Cubic polynomials were used as functions.

The absorptivity model should use the same set of K_i's but with the absorptivity values figured in the range of expected surface temperatures and some constant representative gas temperature used. As with $a_{g,i}$, the $a_{s,i}$ will carry the temperature dependence, and it should be noted from Equations (2.14) and (2.15) that when surface and gas temperatures are equal, $a_{s,i} = a_{g,i}$.

E. Method of Solution

With the emissivity model complete and direct exchange areas available, it is now possible to formulate the radiation balance for the whole enclosure. The leaving flux density W at any surface zone equals the emitted flux εE_s plus reflected flux R. A radiation balance on surface zone i gives

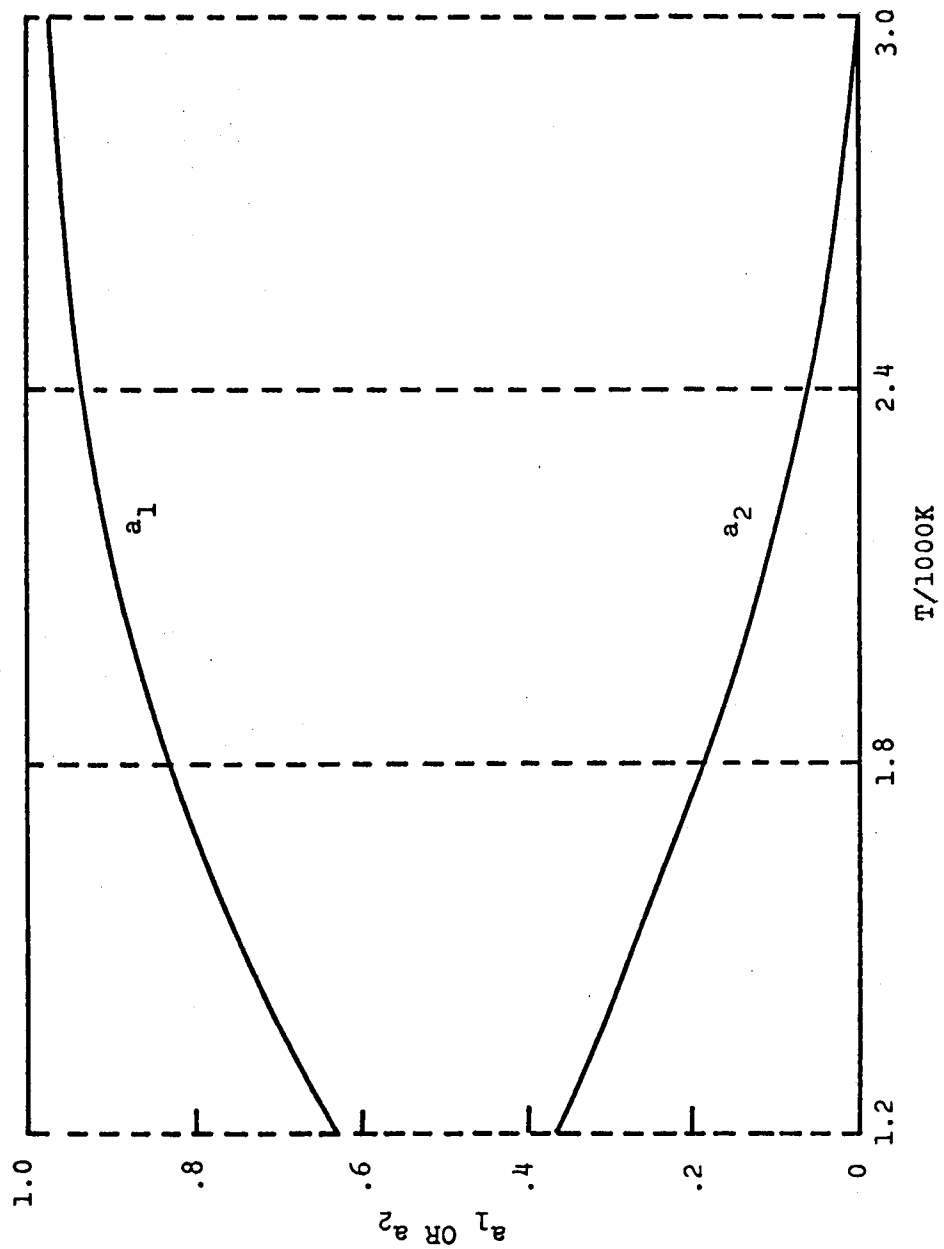


Figure 7. Temperature Weighting Functions.

$$A_i W_i = A_i(\varepsilon_i E_{s,i} + R_i)$$

$$= A_i \varepsilon_i E_{s,i} + \rho_{s,i}\left(\sum_j \overline{s_j s_i}\, W_j + \sum_j \overline{g_j s_i} E_{g,j}\right) \qquad (2.39)$$

or,

$$\sum_j \left(\overline{s_j s_i} - \delta_{ij}\, \frac{A_i}{\rho_{s,i}}\right) W_j = -\frac{A_i \varepsilon_i E_{s,i}}{\rho_{s,i}} - \sum_j \overline{g_j s_i} E_{g,j} \quad . \qquad (2.40)$$

Note that $\overline{s_j s_i} W_j$ represents the radiation streaming away from zone A_j (due to both emission and reflection) that impinges on A_i, and $\overline{g_j s_i} E_{g,j}$ is the radiation emitted by V_j which reaches A_i. The summations thus represent integrations over the whole enclosure. Recall also that the exchange areas are evaluated for a gray gas of uniform concentration throughout the enclosure. The further approximation of gray surfaces is introduced. Now, if there are n surface and m gas zones then the following system of equations results:

$$\begin{bmatrix} \overline{s_1 s_1} - \frac{A_1}{\rho_{s,1}} & \overline{s_1 s_2} & \cdots & \overline{s_1 s_n} \\ \overline{s_1 s_2} & \overline{s_2 s_2} - \frac{A_2}{\rho_{s,2}} & \cdots & \overline{s_2 s_n} \\ \vdots & \vdots & & \vdots \\ \overline{s_1 s_n} & \overline{s_2 s_n} & \cdots & \overline{s_n s_n} - \frac{A_n}{\rho_{s,n}} \end{bmatrix} \cdot \begin{bmatrix} W_1 \\ W_2 \\ \\ \end{bmatrix} = \begin{bmatrix} -\frac{A_1 \varepsilon_1}{\rho_{s,1}} E_{s,1} - \sum_{j=1}^{m} \overline{s_1 g_j} E_{g,j} \\ -\frac{A_2 \varepsilon_2}{\rho_{s,2}} E_{s,2} - \sum_{j=1}^{m} \overline{s_2 g_j} E_{g,j} \\ \\ -\frac{A_n \varepsilon_n}{\rho_{s,n}} E_{s,n} - \sum_{j=1}^{m} \overline{s_n g_j} E_{g,j} \end{bmatrix}$$

Evaluation of the above system yields W_i for the surface zones if temperatures of the zones are known. The net heat flux $q_{net,i}$ at surface zone i is given by

$$q_{net,i} = \frac{\varepsilon_i}{\rho_{s,i}} (E_{s,i} - W_i) \tag{2.42}$$

Thus solution of the W_i allows determination of the net radiative flux at A_i. If i represents a gas zone, the net flux is simply the difference between emission and absorption rates at the zone, i.e.,

$$q_{net,i} = 4 K V_i E_{g,i} - \sum_j \overline{g_j g_i} E_{g,j} - \sum_j s_j g_i W_j \quad . \tag{2.43}$$

Since in most cases the ultimate goal is to find the temperatures, the above system is used instead to solve for what are called "total exchange areas" which are independent of zone temperatures. These represent the net relative radiative exchange between a specified pair of zones. To determine the total exchange area for a pair of zones, one of the zones, say i, is assigned a temperature which will make its black emissive power E_i equal unity, and all other gas and surface zones are assigned temperatures of zero. The system of equations is solved for the W_i and Equations (2.42) and (2.43) are used

to determine the net relative flux. *Upper case letters are used to denote total exchange areas while lower case letters are used for direct exchange areas.* As a consequence of the definition of total exchange areas, the following checks may be applied to them:

$$\sum_{j \text{ incl } i} \overline{S_j S_i} + \sum_{j} \overline{G_j S_i} = A_i \varepsilon_i \tag{2.44}$$

and

$$\sum_{j \text{ incl } i} \overline{G_i G_j} + \sum \overline{G_i S_j} = 4KV_i \quad . \tag{2.45}$$

The above equations, stated in words, say that the emission from a zone i per unit of its emissive power must equal the sum of the total exchange areas between it and all other zones.

With three sets of these total exchange areas available (one for each K_i) it is now possible to calculate what are called "directed flux areas" for each zone pair. This is done by multiplying the total exchange areas by the temperature weighting functions, for example,

$$\overrightarrow{S_i G_j} = a_{s,1}(T_i)\overline{S_i G_j}^1 + a_{s,2}(T_i)\overline{S_i G_j}^2 \quad . \tag{2.46}$$

The arrow above $S_i G_j$ denotes the direction of the flux. In this case surface zone i is the source and gas zone j is the sink. The superscript denotes to which gray gas the total exchange area and temperature function correspond,

and as indicated, that the functions are to be evaluated at the surface zone temperature. The other directed flux area for this pair of zones is given by

$$\overleftarrow{S_i G_j} = a_{g,1}(T_j)\overline{S_i G_j}^1 + a_{g,2}(T_j)\overline{S_i G_j}^2 \qquad (2.47)$$

The gas zone is now the source and the surface zone the sink. The radiative flux between the two elements can now be evaluated as

$$\dot{Q}_{i \rightleftarrows j} = \overrightarrow{S_i G_j}\, E_i - \overleftarrow{S_i G_j}\, E_j \quad . \qquad (2.48)$$

The problem of determining the temperature field and heat flux distribution for the enclosure is reduced to an iteration procedure between this equation and an equation relating heat loss to flame temperature. The first set of trial temperatures could be adiabatic flame temperatures for the gas zones, and some predetermined set of wall temperatures. After subtracting heat losses from the available enthalpies of their respective gas zones, a second set of temperatures would be calculated and the whole procedure repeated.

It is important to note that only for surface to surface exchange will the clear gas temperature function $a_{s,3}(T_s)$ be needed since a gas of K = 0 would be non-participating. The form of the directed flux areas for surface to surface exchange will be

$$\overrightarrow{S_iS_j} = a_{s,1}(T_i)\overline{S_iS_j}^1 + a_{s,2}(T_i)\overline{S_iS_j}^2 + a_{s,3}(T_i)\overline{S_iS_j}^3 \quad ,$$

$$\overleftarrow{S_iS_j} = a_{s,1}(T_j)\overline{S_iS_j}^1 + a_{s,2}(T_j)\overline{S_iS_j}^2 + a_{s,3}(T_j)\overline{S_iS_j}^3 \quad .$$

(2.50)

Gas to gas directed flux areas are evaluated in a similar manner, using the a weighted total exchange areas for each radiating component, as follows:

$$\overrightarrow{G_iG_j} = a_{g,1}(T_i)\overline{G_iG_j}^1 + a_{g,2}(T_i)\overline{G_iG_j}^2 \quad , \tag{2.51}$$

$$\overleftarrow{G_iG_j} = a_{g,1}(T_j)\overline{G_iG_j}^1 + a_{g,2}(T_j)\overline{G_iG_j}^2 \quad . \tag{2.52}$$

The reasoning behind the form of the emissivity function now becomes apparent. In the form of Equation (2.30) it can be used to represent a flame of nonuniform temperature where emissivity is temperature dependent, in calculations of the preceding type. A convective heat transfer coefficient should now be estimated for the outside volume to surface contact. For the purposes of this program a formula from Reference [8] is used,

$$\frac{hD}{k} = 0.021\ Pr^{0.6}\ Re^{0.8} \tag{2.53}$$

where

h = convection coefficient,

D = diameter of combustor,

k = thermal conductivity of gaseous mixture,

Pr = Prandtl number of gaseous mixture,

Re = Reynolds number of gaseous mixture.

This completes the calculational procedure for the zone heat transfer method.

CHAPTER III

CALCULATIONS USING ZONE METHOD

A. Required Inputs

A computer program using the procedure discussed in Chapter II was written for this work. The results are printed out as the total rate of loss or gain of energy for each zone. Since this is a steady state problem, the sum of all the rates of gain for the enclosure must equal zero, losses being negative.

Input information required to run a specific case is as follows:

1. Surface zone temperatures and emissivities.
2. Gas zone temperatures and properties of flame.
   a. Partial pressure of CO_2.
   b. Partial pressure of H_2O.
   c. Partial pressure of CO.
   d. Average coal particle size (input).
   e. Fraction volatile matter in coal.
   f. Residence time.
   g. Coal flow rate.
   h. Total combustor pressure.

1. Surface temperatures and emissivities. The surface zone temperatures, except for the end zones, can be taken to be the temperature of liquid coal slag of a certain minimum viscosity since slag is known to coat the walls during the operation. The dominant factor in the radiant heat transfer is gas temperature, so that surface temperatures are not as critical to the overall heat losses. Reference [10] shows slag flowing temperatures of 2500-2900°F being common for most coal slags. Surface temperatures around 1700K would seem reasonable in the light of this information. Wall emissivities of around 0.8 seem reasonable in this temperature range. References put emissivity of iron oxide at temperatures above 2000°F at about 0.9 with alumina and silica mixtures considerably less.

The end surface zones pose a problem in that, except in the case of the perforated injection plate, they are not real surfaces but only imaginary boundaries. The upstream end has oxygen and nitrogen enriched products of kerosene combustion entering at about 1300K. Since this mixture is comparatively transparent to radiation but is backed by real surfaces at varying distances, some sort of effective emissivity will have to be estimated. Likewise the

downstream end surface zones are imaginary and effective emissivities will need to be calculated for them. At this end, however, the flame is hotter, optically more dense, and the backing surfaces are much closer. It was stated earlier that these problems would require some thought and the results some interpretation.

2. Gas temperatures and flame properties.

A systematic approach is needed for getting, at least, the adiabatic flame temperatures for the gas and downstream end zones, as well as chemical analysis for a given set of inputs such as total pressure, fuel and oxidizer compositions and flow rates. Arora [4] let a certain proportion of coal be burned for each axial division in his combustor model. By utilizing the computer program of Reference [1], he obtained adiabatic flame temperatures for each of 10 axial segments with 10 percent of char (fixed carbon) burned in each. Tables 2 and 3 show his results for 2 sets of input conditions, though neither correspond to the 5.5 atm total pressure and 85 percent theoretical (fuel rich) 1300 K oxidizing mixture of N_2,O_2 and kerosene combustion products which correspond to the inputs of the combustor under study. Neither do Arora's results attempt to show any radial variation of temperature. The computer program of Reference [1] has been used, however, to get the partial pressures of the gases and an

TABLE 2

VARIATIONS ALONG CHAMBER LENGTH, P = 4 (atms), E_R = 1.0
(OXIDIZER: ORDINARY AIR AT 1,900°K)

Segment No.	Percent of Char Burned	Adiabatic Flame Temperature (°K)	Molecular Weight of Gases	Cp $\left(\frac{\text{cal.}}{\text{gm °K}}\right)$
1	10	2704	30.287	0.6319
2	20	2724	30.196	0.6563
3	30	2743	30.102	0.6799
4	40	2760	30.004	0.7023
5	50	2775	29.903	0.8244
6	60	2790	29.800	0.8446
7	70	2803	29.694	0.8627
8	80	2814	29.587	0.8785
9	90	2825	29.471	0.8920
10	100	2835	29.366	0.9030

Fuel: TVA Coal

Seed: K_2CO_3 (1.2% K of total reactants)

PVM = 60%

(Note: All volatiles are assumed to burn in first segment.)

TABLE 3

VARIATIONS ALONG CHAMBER LENGTH, P = 4 (atms), E_R = 1.0
(OXIDIZER: PURE O_2 at 298 °K)

Segment No.	Percent of Char Burned	Adiabatic Flame Temperature (°K)	Molecular Weight of Gases	Cp $\left(\frac{\text{cal.}}{\text{gm °K}}\right)$
1	10	3112	35.781	1.5500
2	20	3132	33.300	1.6500
3	30	3151	32.836	1.7300
4	40	3168	32.371	1.7840
5	50	3183	31.915	1.8400
6	60	3197	31.467	1.8920
7	70	3210	31.027	1.9360
8	80	3222	30.596	1.9740
9	90	3233	30.174	2.0070
10	100	3243	29.760	2.0356

Fuel: TVA coal

Seed: K_2CO_3 (1.2% K of total reactants)

PVM = 60%

(Note: All volatiles are assumed to burn in first segment.

upper limit on the temperature of the flame. Gas temperatures cannot be much greater than the adiabatic flame temperature at chemical equilibrium.

It is possible by running the heat transfer program with some trial temperature distributions to get a feel for what temperatures are required to produce a given heat flux distribution. Since no model is available which gives oxidizer and fuel mixing patterns, thus radial as well as axial temperatures, it is felt that the above approach should be used until something more comprehensive can be developed. The input gas zone temperatures used up to this time, therefore, have been estimated purely from the experience of having run the program many times.

B. Demonstration of the Method

In order to demonstrate the program the data from two experimental combustor tests are utilized as follows. The actual conditions and heat flux distributions of the two runs are tabulated first. This is done in Table 4. Next the program of Reference [1] is run for the equilibrium combustion of the input flows and pressure. Table 5 shows the results for Run 36-4. The other run gives almost exactly the same adiabatic flame temperatures and other properties. Note that the properties have been calculated over a range of total pressures. It is necessary to choose the properties corresponding to the estimated combustion

TABLE 4

RUN CONDITIONS AND HEAT LOSSES
FOR RUNS 36-4 AND 36-33

		RUN 36-4 (w/o plate injector)	RUN 36-33 (w/ plate injector)
$\dot{m}_{coal}$		1.05 #/sec	1.03 #/sec
$\dot{m}_{seed}$		0.105 #/sec	0.103 #/sec
$\dot{m}_{kerosene}$		0.11 #/sec	0.10 #/sec
$\dot{m}_{O_2}$		2.41 #/sec	2.25 #/sec
$\dot{m}_{N_2}$		0.42 #/sec	0.40 #/sec
$\dot{m}_{total}$		4.095 #/sec	3.883 #/sec
P_{total}		5.5 atm	5.5 atm
Losses:			
Surface 1 + Surface 2	PP*		7500 BTU/min
Surface 5	CS†	1000 BTU/min	4500 BTU/min
Surface 6	CS†	1150 BTU/min	13000 BTU/min
Surface 7	CS†	1150 BTU/min	21000 BTU/min
Surface 8 + $\frac{1}{4}$ Surface 9	CS†	1800 BTU/min	14750 BTU/min

*Perforated plate.

†Cylindrical section.

TABLE 5

EQUILIBRIUM THERMODYNAMIC PROPERTIES AND CHEMICAL COMPOSITION OF COMBUSTION PRODUCTS FOR RUN 36-4

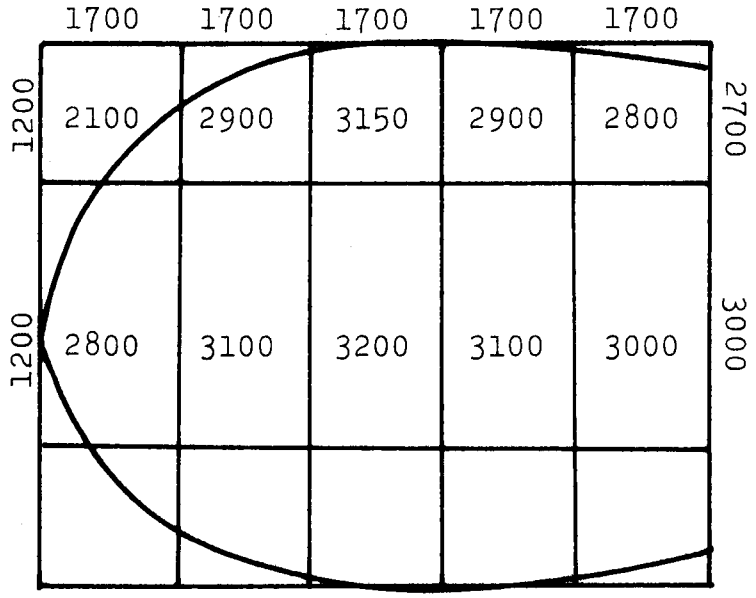
Thermodynamic Properties					
P, ATM	4.0000	4.5000	5.0000	5.5000	6.0000
T, DEG K	3101	3115	3127	3138	3148
RHO, G/CC	4.5448-4	5.0973-4	5.6484-4	6.1981-4	6.7465-4
H, CAL/G	-386.5	-386.5	-386.5	-386.5	-386.5
S, CAL/(G)(K)	2.4160	2.4079	2.4007	2.3942	2.3882
M, MOL WT	28.912	28.950	28.983	29.014	29.042
CP, CAL/(G)(K)	1.6739	1.6508	1.6304	1.6121	1.5955
GAMMA (S)	1.1157	1.1162	1.1167	1.1171	1.1175
SON VEL,M/SEC	997.5	999.2	1000.8	1002.2	1003.5
CND, MHO/M	3.2451 1	3.1155 1	3.0000 1	2.8960 1	2.8017 1
Mole Fractions of Constituent Gases in Combustion Products					
O2	.04073	.04024	.03979	.03938	.03901
CO2	.23489	.23609	.23718	.23818	.23910
H2O	.19758	.19832	.19898	.19959	.20014
N2	.10136	.10145	.10154	.10162	.10169
CO	.27222	.27167	.27118	.27071	.27029
NO	.00881	.00890	.00897	.00904	.00910
SO2	.00901	.00902	.00903	.00905	.00906
H2	.03100	.03080	.03062	.03045	.03030

pressure of the run being considered, in this case 5.5 atm.

The mole fractions of the gases are used to determine the partial pressures of CO_2, H_2O and CO which are used as inputs to the heat transfer program. A convection heat transfer coefficient is estimated for the walls of the combustor and for the perforated plate when used. Finally a gas zone temperature distribution is guessed and the program is run.

By running the heat transfer program with several trial input temperature distributions, heat loss versus axial length distributions are obtained which compare reasonably with measured losses. The resulting losses using the temperature distributions of Figure 8 are compared to actual losses in Figures 9 and 10. Obviously there is no proof that these temperature fields actually exist during operation of the combustor, but they do correspond to a situation which, subject to the simplifications and approximations stated so far, could produce the measured losses. Again it is pointed out that in the absence of flow models which give burning patterns this is probably as good a result as can be expected. In Figure 11 isotherms are drawn which yield approximately the average zone temperatures of Figure 8.

WITH WATER COOLED INJ. PLATE (RUN 36-33)



WITHOUT PLATE (RUN 36-4)

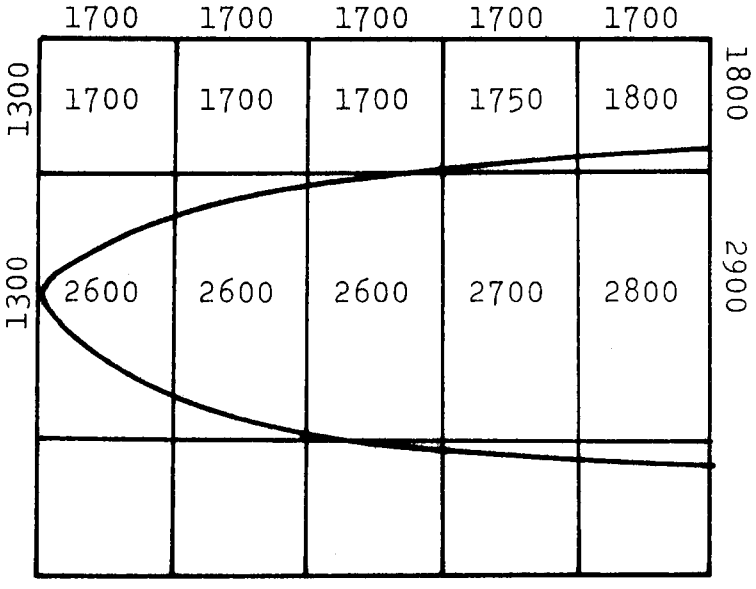


Figure 8. Input Zone Temperature.

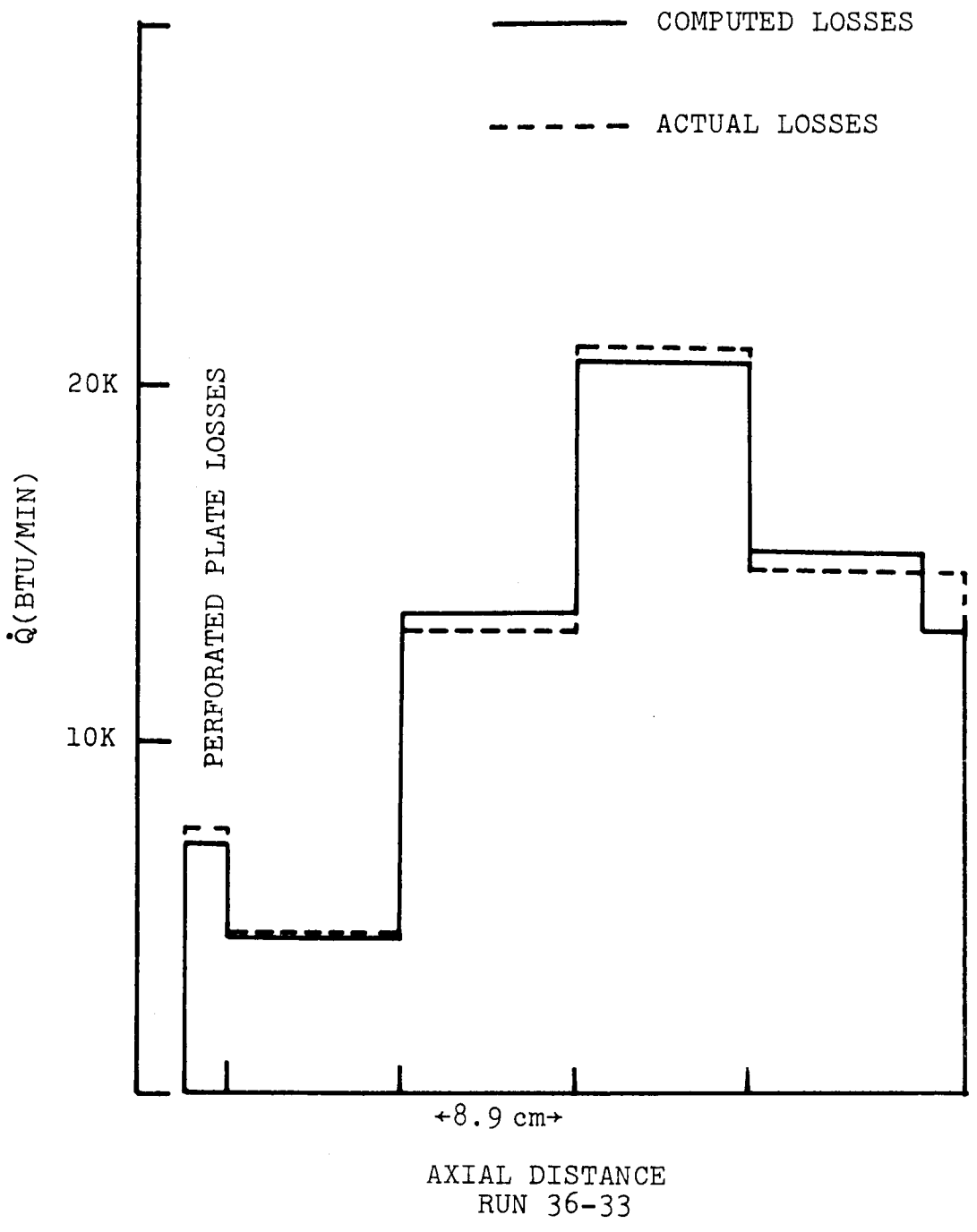


Figure 9. Actual and Computed Losses for Run 36-33.

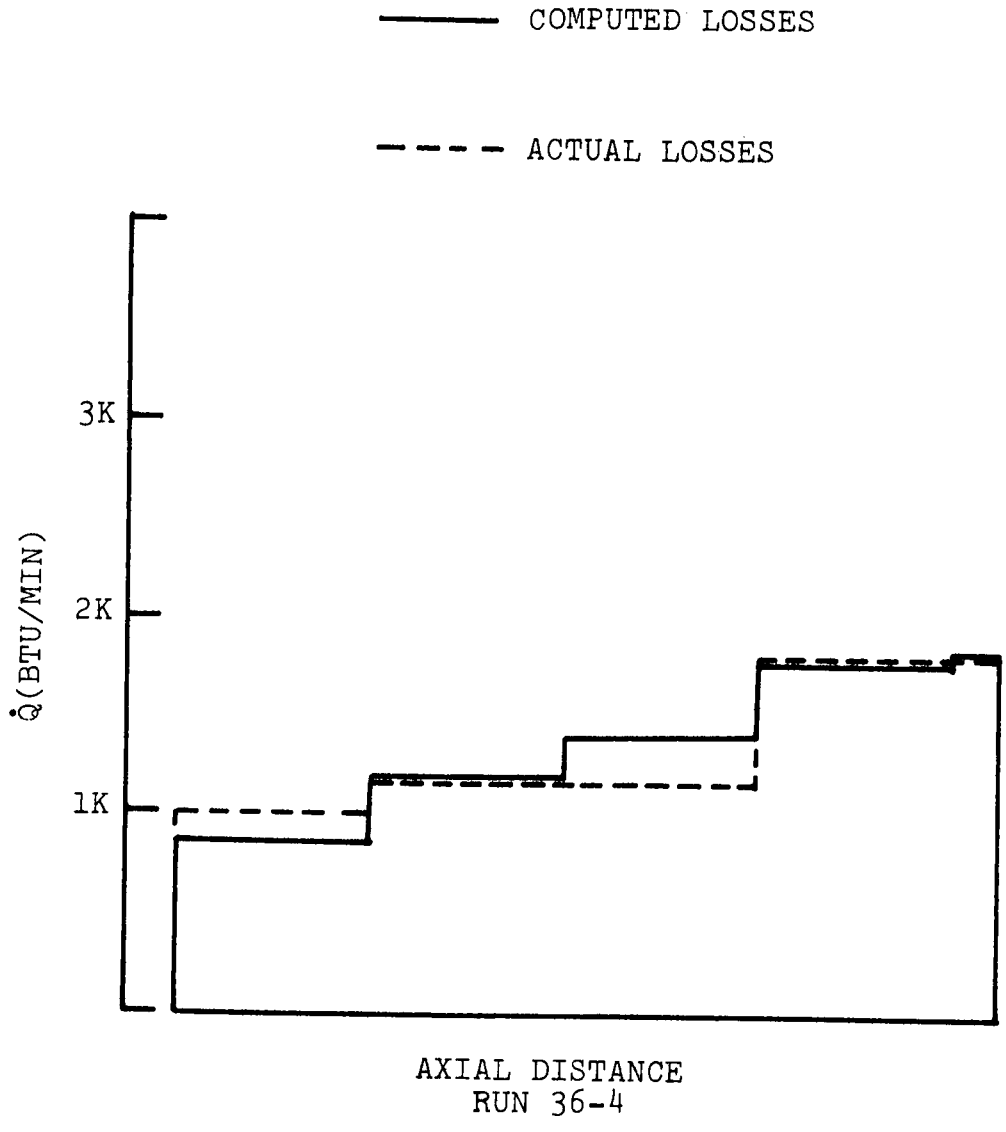
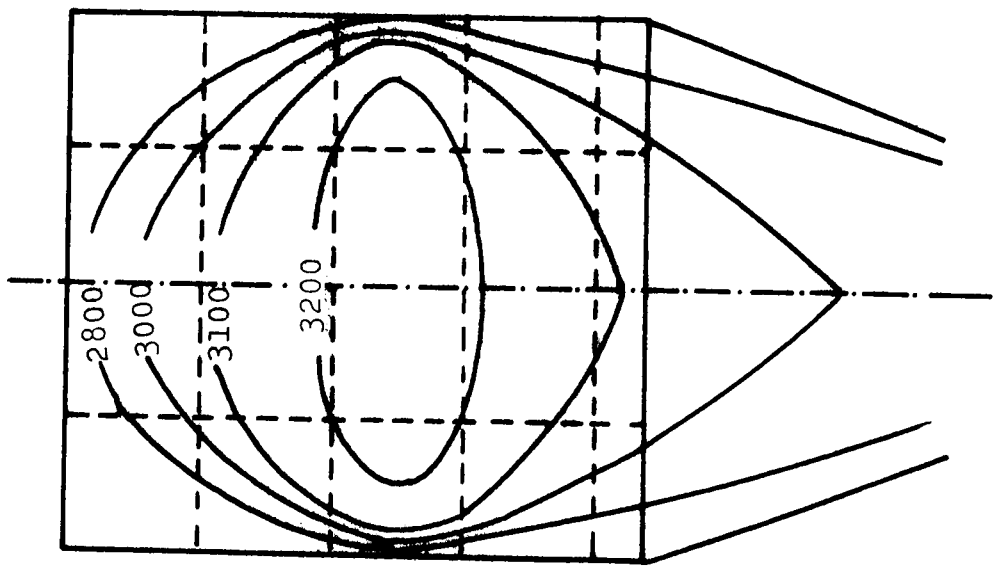
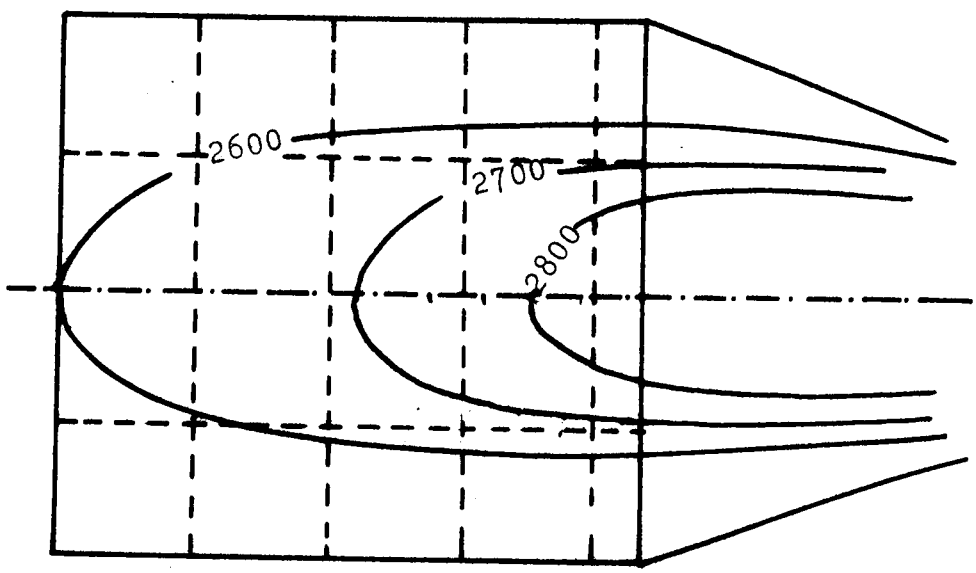


Figure 10. Actual and Computed Losses for Run 36-4.



RUN 36-33



RUN 36-4

Figure 11. Theoretical Temperature Fields.

CHAPTER IV

DISCUSSION OF RESULTS

The theoretical temperatures estimated for the poorly mixed case (Run 36-4) seem likely to contain more error than those for the well mixed case. First of all, the computed axial losses are not as close to the actual losses as they are in the other run. Secondly, due to the poor mixing, the constant composition approximation is more doubtful. Instead of being modeled as a uniform composition cloud, a more accurate model would possibly have used a very dense central core of high emissivity and somewhat lower temperature, surrounded by a more transparent and hotter envelope of gases.

The temperatures from Run 36-33 seem unrealistically high in the central region and also could be explained on the basis of nonuniform composition. The particles, which control emissivity to a large extent, are likely to be more concentrated in the central region, thus increased emissive power could be obtained even with slightly lowered temperatures. Likewise, greater energy transport from central regions to walls would be attained with a more transparent medium in the intervening space. This is one of the shortcomings of this simplified model,

that it assumes constant composition, though not temperature, of the combustion products.

Data from the two runs being studied here show that heat transfer from the well mixed run continues to be higher than that of the other run until the throat of the nozzle is reached. Gas analysis data from even further downstream shows that significant oxygen is present in the products of the poorly mixed combustion of Run 36-4. Indications are that the mean gas temperature from 36-33 peaks in the combustor section, then falls off as the gases move downstream. In the poorly mixed run, on the other hand, it is felt that combustion is continuing in the conductivity channel. Neither case seems to represent an optimum condition, from the standpoint of power production.

CHAPTER V

CONCLUSIONS AND SUGGESTIONS FOR FURTHER WORK

As it now stands the heat transfer program developed from this work is rather limited in its application. A number of improvements are possible, at present, which would not require a great deal of time and effort on the part of anyone interested in using it.

One obvious improvement would be a refining of the mesh. Nondimensional exchange areas are available for cylindrical geometry from Reference [3] which would enable the enclosure to be divided up into 12 axial segments with 5 radial cores. If done, an added benefit would be a raising of the limit on K_i, consequently a better emissivity model.

Another improvement would be a better representation of burning particles. Only the simplest possible approach is used in this work. Reference [4] contains a more thorough treatment of particle combustion history. In this work coal and seed (K_2CO_3) particles have been lumped together when they could have been treated separately, with presumably greater accuracy. Soot emissivity has not been considered in the model. Soot particles (much smaller than char particles considered here) cannot be treated with the same approach as used

in larger char particles. Reference [3] contains information on how soot emissivity can be estimated.

In the long run, it would be beneficial to allow for nonuniform composition of the cloud, though this would greatly complicate the calculational procedure. Reference [3] offers some guidelines for incorporating this feature into the method. Nonuniform composition (K_i dependent on location) would allow two gas zones of equal temperature to emit-absorb-transmit differently, as is thought to be the case where particle and gas streams are poorly mixed.

With the above improvements made, and a compatible zone mixing model along with the already available computer program of Reference [1], the means for accurately predicting temperatures and losses would become available. This goal, thus achieved, would enable designers of future combustors to develop optimum designs for commercial applications.

LIST OF REFERENCES

LIST OF REFERENCES

1. Gordon, Sanford, and Bonnie J. McBride. "Computer Program for Calculation of Complex Chemical Equilibrium Compositions, Rocket Performance, Incident and Reflected Shocks, and Chapman-Jouquet Detonations," NASA SP-273, 1971.

2. Postlethwaite, A. W., and M. M. Sluyter. "Heat Transfer Problems Associated with an MHD Power Generation System--An Overview," ASME Paper No. 77-HT-62 (also see [9]).

3. Hottel, H. C., and A. F. Sarofim. Radiative Transfer, McGraw-Hill Book Company, Inc., New York, 1967.

4. Arora, Balbir. Ph.D. Dissertation in Mechanical Engineering, The University of Tennessee, Knoxville, 1976.

5. Roy, Gabriel. Written communication from, July 1978.

6. Ludwig, C. B., W. Malkmus, J. E. Reardon, J.A.L. Thomson. Handbook of IR Radiation from Combustion Gases; R. Goulard and J.A.L. Thomson, Eds., NASA SP-3080, 1973.

7. Kolbe, Ronald L. Written communication from, May 1978.

8. Kays, W. M. Convective Heat and Mass Transfer, McGraw-Hill Book Company, New York, 1966.

9. Sarofim, A. F., J. B. Howard, A. Padia, and H. Kobayashi. "Heat Transfer and Kinetic Limitations in the Design of Single-Stage Coal Fired Combustors for Open-Cycle MHD Generators," Sixth International Conference on Magnetohydrodynamic Electrical Power Generation, Vol. II, Washington, D.C., 9-13 June, 1975.

10. Sage, W. L., and J. B. McIlroy. "Relationship of Coal Ash Viscosity to Chemical Composition," Combustion, November 1959, p. 42.

VITA

The author was born on November 10, 1950, in San Antonio, Texas, to Allen and Waneta Carlson. He received his high school diploma from North Salinas High School, Salinas, California, in June 1968, and was married to the former Sonja Vincent on October 23, 1971. From June 1968 until January 1975 he worked both full and part-time at a number of jobs, mostly factory type work, and took college courses as the situation permitted.

In January 1975 he entered Middle Tennessee State University as a full-time student, where he was able to complete his undergraduate requirements.

He received his B.S. degree from MTSU in May 1977, satisfying requirements for majors in Physics and Mathematics and a minor in Industrial Technology. Upon graduation he enrolled at The University of Tennessee Space Institute to pursue the M.S. degree and work as a Graduate Research Assistant in the Energy Conversion Division.